Eur. Phys. J. D **13**, 51–59 (2001)

THE EUROPEAN PHYSICAL JOURNAL D

EDP Sciences

Intermediate energy (e, 2e) processes on C_{60}: A distorted wave Born approximation study

S. Keller[a]

Institut für theoretische Physik, Universität Frankfurt, 60054 Frankfurt, Germany

Received 14 April 2000 and Received in final form 27 July 2000

Abstract. Triple differential cross-sections (TDCS) for $(e, 2e)$ processes on C_{60} have been calculated in the plane wave Born and distorted wave Born approximations using a jellium shell model to describe the target valence states. The peculiarities of these TDCS are demonstrated by comparison with results for atomic hydrogen. Ionisation into a resonant state leads to dramatic modifications of the TDCS. This effect could also be observed in a surface $(e, 2e)$ experiment in specular geometry using a thin film of physisorbed C_{60}.

PACS. 34.80.Gs Molecular excitation and ionization by electron impact

1 Introduction

The beauty of the highly symmetric fullerene molecule C_{60} continues to fascinate the physics community. Therefore, since its discovery this system has been studied using the full spectrum of experimental techniques available to date. For instance, electron momentum (or $(e, 2e)$) spectroscopy has been used to determine the momentum density of states of C_{60} [1]. Like in any $(e, 2e)$ experiment, in this study the triple differential ionisation cross-section (TDCS) was measured by detecting the two outgoing electrons in coincidence resolved in energy and solid angle. The kinetic energies of all continuum electrons were chosen so large (several keV, to be compared with ionisation potentials of a few 10 eV) that the experimental data could be interpreted assuming the ionizing process to be simply a quasi-free binary electron-electron collision. Under these conditions the TDCS turns out to be a direct map of the single-particle initial state wave function [2].

In contrast, at lower impact energies (well above the ionisation threshold, but within the same order of magnitude) the $(e, 2e)$ TDCS is known to carry signatures not only of the initial bound state of the target, but also of the structure of the target continuum and the dynamics of the ionisation process itself [3]. Given this complexity, and the large body of results from other scattering experiments already available, it is fair to ask whether $(e, 2e)$ experiments on fullerene at these intermediate impact energies could deliver any new and useful insights at all. It is the main purpose of the present study to give a (preliminary) answer to this question. To this end, the remainder of this introduction summarizes some previous results on scattering from fullerene and fullerene ionisation. Section 2 outlines the model underlying the calculations reported in Sections 3 and 4. Atomic units are used throughout this paper.

Characteristics of electron scattering from fullerene

There are three phenomena characteristic for electron scattering from clusters in general and from fullerene in particular. All of them are essentially due to the presence of a delocalised multi-electron system confined to a geometrically well-defined volume. Firstly, the global geometrical constraint of the fullerene cage structure is directly mapped into oscillations in the elastic electron scattering [4] (and photoionisation [5]) cross-sections. Corresponding oscillations have also been observed in TDCS for the (e, ep) process of nuclear physics [6]. It can therefore be expected that this type of signature will also show up in $(e, 2e)$ TDCS [7]. The relations between these phenomena are discussed in Appendix A.

Secondly, it was recognized quite early that the delocalisation of the valence electrons in fullerenes should allow for collective excitations [8]. Electron energy loss spectroscopy (EELS) of C_{60} has indeed unambiguously established the existence of a π plasmon at about 6 eV and a broad σ plasmon at about 15 eV, as well as evidence for another π plasmon at 28 eV [9–11]. Theoretically, the response properties of fullerene have been discussed in [8,11–14] using methods ranging from semi-phenomenological ansatzes to full-fledged many-body perturbation theory. These studies consistently provide good agreement with the experimental data. It is thus fair to say that this aspect of inelastic electron scattering on fullerene is reasonably well understood.

Thirdly, again drawing on the analogy between clusters and atomic nuclei [15], one would anticipate the existence of both Feshbach and shape resonances in the effective

[a] e-mail: keller@th.physik.uni-frankfurt.de

potential well formed by the carbon nuclei and core electrons. To date, the most explicit experimental evidence of this effect is the observation of pronounced structures in the cross-section for electron attachment to neutral C_{60} at impact energies below 10 eV [16,17]. Hints at the existence of resonances were also found in the EELS experiment of [9] discussed above. These authors observed variations of the EELS peak intensities at energies between 2 and 10 eV that could be due to shape resonances. A similar interpretation of structures in the elastic scattering data of reference [18] has been proposed in [19]. Indeed, various methodically different calculations predict the existence of shape resonances in the cross-section for elastic electron scattering from C_{60} [19,20], but there is no consensus about their number and position.

From this overview of previous results, it is obvious that while much is known about the global response properties of fullerene, our understanding of the positive-energy states of these systems is still rudimentary. The present paper introduces the $(e, 2e)$ technique as a means to investigate this problem.

2 Theoretical model

2.1 Jellium sphere model of C_{60}

All calculations reported in the present study are based on the spherical jellium shell model of C_{60}. This model was first proposed in references [12,21] as a means to analyze the optical response of fullerenes. It approximates the potential generated by the carbon nuclei and the $1s$ electrons by a spherical potential well of radius 6.7 Å and thickness 5.6 Å. The depth of this well is defined in the spirit of the jellium model of metal clusters [22]. To obtain the effective single particle orbitals from this model, the corresponding ground state Kohn-Sham equations of density functional theory [23] were self-consistently solved with this external ionic potential using a Latter correction to force the proper $-1/r$ asymptotic behaviour of the self-consistent effective potential. Further details are given in [24]. Due to the spherical symmetry, the resulting ground state wave function is represented by only 15 effective one-electron orbitals, with quantum numbers in the range $n = 1, 0 \leq l \leq 9$ and $n = 2, 0 \leq l \leq 4$. Figure 1 shows the effective potential and the corresponding bound state orbitals and eigenvalues.

By comparison with the experimental data of reference [1], it was shown in [24] that this model provides a reasonable starting point for investigating $(e, 2e)$ on C_{60} if a representation of the quasi-continuum of valence states by discrete levels is acceptable. Figure 1 shows that the shape differences between the radial wave functions for different angular momenta but same principal quantum number are marginal. In order to discuss the dominant features of the corresponding $(e, 2e)$ TDCS, it is therefore sufficient to consider only the $1s$ orbital (binding energy 1.25 a.u.). This state is most convenient for comparison with atomic data (see Sect. 3.1).

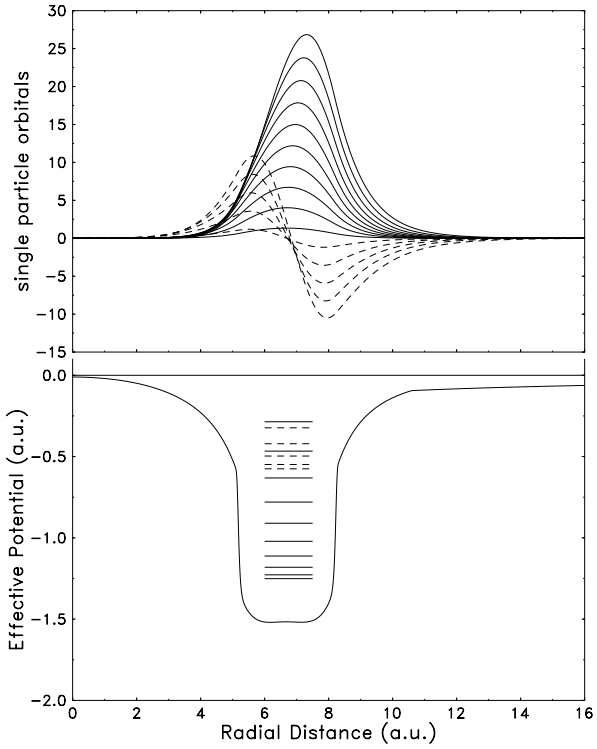

Fig. 1. Effective self-consistent potential, bound state orbitals and eigenvalues (indicated by straight lines in the potential well) for the spherical jellium sphere model of C_{60}. Full curves: $n = 1$ manifold, dashed curves: $n = 2$ manifold.

2.2 First-order theories of electron impact ionisation

The plane wave Born (PWBA) and distorted wave Born (DWBA) models are the only standard models currently available for the calculation of $(e, 2e)$ TDCS on many-electron targets. The basic assumption of these theories is that the ionisation is due to the exchange of a single virtual photon between the two active electrons. The explicit form of the relevant scattering amplitudes have repeatedly been discussed in the literature (see, *e.g.*, [25] for the PWBA and [26] for the DWBA), so a very brief outline will be sufficient here.

The $(e, 2e)$ TDCS for ionisation of a closed shell (characterized by a set b of quantum numbers) can be written as

$$\frac{\mathrm{d}^3\sigma_{(e,2e)}}{\mathrm{d}E\,\mathrm{d}\Omega_1\mathrm{d}\Omega_2} = 2(2\pi)^4 \frac{k_1 k_2}{k_0} \left|T\left(\mathbf{k}_0, \mathbf{k}_1, \mathbf{k}_2, b\right)\right|^2 . \quad (1)$$

Using standard scattering theory, the first order T matrix $T^{(1)}$ is found to read

$$T^{(1)}\left(\mathbf{k}_0, \mathbf{k}_1, \mathbf{k}_2, b\right) = \left\langle \psi^{(-)}_{k_1}(\mathbf{x})\phi^{(-)}_{k_2}(\mathbf{y}) \left|\right| \mathbf{x} - \mathbf{y} \left|^{-1}\right| \psi^{(+)}_{k_0}(\mathbf{x})\phi_{\mathrm{b}}(\mathbf{y}) \right\rangle \quad (2)$$

where antisymmetrization of the product wave functions $\psi(\mathbf{x})\phi(\mathbf{y})$ of the two active electrons is understood. The standard notation for incoming and outgoing spherical wave boundary conditions has been used, and (in the direct amplitude) indices 0, 1 and 2 label the momentum

of the incoming, the scattered and the outgoing electron state, respectively.

The DWBA as used in the present work is obtained by calculating all wave functions using the effective (long-ranged) potential representing the target nuclei and spectator electrons (see below). For the case of the hydrogen atom, this model is equivalent to the standard Coulomb-Born approximation. Assuming the effect of the potential on the projectile states ψ to be negligible, one arrives at the PWBA. The choice of the same potential in both initial and final channels renders all wave functions orthogonal, so that there is no perturbative projectile elastic scattering contribution to the FBA amplitude.

While the calculation of the PWBA amplitudes is completely straightforward, the evaluation of the DWBA amplitudes for C_{60} proves to be a more formidable task due to the slow convergence of the partial waves series for the scattered electron caused by the large spatial size of the target. To efficiently deal with this problem, for the present study a new DWBA computer code was developed from scratch (except for use of the wave equation solver described in Ref. [27]). Extensive tests against CBA and DWBA results for atoms published by different groups were carried out to verify this code. The residual error due to incomplete convergence was estimated by comparing results of calculations with different numbers of partial waves. Except when otherwise stated, in the DWBA results for C_{60} given below it is significantly smaller than 10%.

2.3 Many-body effects and effective scattering potentials

From the experimental results mentioned in the introduction, it is obvious that many properties of fullerene are due to many-body effects. It is therefore important to clarify to what extent such effects are incorporated in the present calculations, which according to equation (2) are based on the notion of single-particle orbitals.

By construction, many-body effects can only enter single-particle orbitals *via* an effective one-body potential. Formally, the effective potential including the dynamical response of the entire many-electron systems is well defined in terms of the many-body self-energy. In the PWBA, the self-energy of the target alone may be used because the projectile is treated as an external perturbation Therefore in this case, there is also a direct relation between the differential inelastic electron scattering cross-section and the polarization propagator of the target system (see, *e.g.*, [28]). An application of this approach to electron scattering on C_{60} has been reported in [29]. Unfortunately, as will be evident from the numerical results given below, the PWBA is not reliable at the impact energies considered here. This implies that an analysis of the Dyson equations describing the propagation of the target states *and* the projectile electron is required to construct the self-energy required. This approach amounts to a coupled-channel description of the entire system. Unfortunately, to date such calculations are prohibitively complex even for small molecules if the impact energy significantly exceeds the ionisation threshold so that many reaction channels are open.

In practice, it is therefore a common procedure to mimick the response of many-electron targets by model exchange and polarization potentials derived from phenomenological arguments and basic considerations of many-body perturbation theory (see, *e.g.*, [30–32]). While reasonable for intermediate energies, this approach becomes questionable for low-energy continuum electrons. This has been demonstrated for the case of elastic scattering of low-energy electrons on jellium spheres (an idealization of alkaline clusters), where it was found that the choice of the model exchange and polarization potentials strongly affects the calculated cross-sections [33]. Hence it must be acknowledged that the model potential approach is not sufficiently well understood to be routinely used as input for studies of scattering on cluster targets. This implies that to date there is no computationally efficient standardized strategy for describing the response of a fullerene target to an additional continuum electron in terms of an effective scattering potential.

In view of this difficulty, the present paper resorts to formal consistency as the guiding principle in the definition of an effective one-body potential. As stated above, the main model assumption used in this work is that only a single virtual photon is exchanged between the active electrons. Hence all active single electron states have to be described taking into account the interaction with the residual ion only. As a second approximation, it is assumed that the residual ion is passive, *i.e.* its state can be described by a one hole-configuration of the neutral system. This implies that the effective potential used for describing the initial bound state should also be used for describing all scattering states.

The effective potential used in this work is the output of a DFT structure calculation which includes the exchange interaction between the target valence electrons [24]. Therefore if ejected electron states (which are states in the ionic continuum) are calculated from this potential, exchange effects are taken into account using the standard local exchange approximation frequently used in scattering calculations [32]. Asymptotically, by virtue of using the Latter correction the DFT potential is the potential "seen" by a target electron removed to a large distance from the jellium shell. In this situation, polarization effects are not of primary importance because outside the target, the effective potential is dominated by the long-ranged monopole Coulomb potential of the residual ion. By construction, the same effective potential is also to be used for the scattering states of the projectile. For these high energy states, the assumption of a frozen ionic core is even more appropriate. Notice also that again, exchange with the spectator electron states is described in terms of a local exchange approximation.

Evidently, the simplistic description of the influence of many-body effects on low-lying continuum states is the main limitation of the first order model used in this work. Moreover, resonant excitation of the target to an

autoionising state (see [34] and references therein, note also [35]) could significantly alter shape and magnitude of $(e, 2e)$ TDCS by interference between direct and resonant amplitudes. This many-body effect is also not included in the present study. However, it is obvious that these defects can only be remedied by some sort of nonperturbative approach to the general problem of electron-cluster scattering, which is outside the scope of the present exploratory study.

3 Numerical results

In this section, the three specific features of inelastic scattering on C_{60} mentioned in the introduction, are discussed in the context of intermediate energy $(e, 2e)$ physics.

3.1 Standard (e, 2e) kinematics and oscillations of the TDCS

There are three standard kinematical arrangements that have extensively been studied for $(e, 2e)$ on atomic targets. While all of them are coplanar, *i.e.* all electron momenta are in the same plane, they highlight different aspects of the scattering process. In the following, predictions for $(e, 2e)$ TDCS on the $1s$ state of the jellium shell model of C_{60} in these geometries will be confronted with standard numerical results for atomic hydrogen in order to bring out the peculiarities to be expected when studying cluster targets. Following Ehrhardt *et al.* [36], all energies are scaled with the ratio of the binding energies to allow for comparison of the different target systems.

3.1.1 Ehrhardt geometry, small perturbation

In the coplanar asymmetric geometry, the two outgoing electrons are detected at very much different energies, so that with high probability the fast electron is the scattered one. Keeping its detection angle fixed and measuring the TDCS as a function of the detection angle of the slow electron ("Ehrhardt geometry"), one essentially studies the response of the target to a well-defined perturbation. Obviously, the PWBA is a useful model for this situation if the perturbation (represented by the momentum transferred to the target) is small and the exchange amplitude can be neglected [36]. At very small perturbations, one approaches the photoionisation limit, so that the ionisation process can be characterized by the dipole oscillator strength [37,38].

Numerous experiments using this geometry have been carried out by Ehrhardt and collaborators on atomic hydrogen targets [36,39]. They confirm the gross structure of the calculated TDCS shown in Figure 2a for one representative case. The TDCS is dominated by transitions due to absorption of a (virtual) dipole photon. Hence the TDCS for ionisation of the initial s state clearly shows a dipole pattern centred around the direction of momentum transfer. The discrepancies between FBA and DWBA (*i.e.* CBA) data are only quantitative, illustrating the statement that projectile rescattering plays no significant role here.

The situation is completely different for the jellium shell model. By construction, the PWBA data still show the symmetry of the TDCS with respect to the direction of momentum transfer, but the dipole pattern is replaced with a more complex shape, indicating that even at small momentum transfers, higher angular momentum states are populated. Indeed, additional calculations show that the dipole pattern only re-emerges at very small momentum transfers ($\ll 0.1$ a.u.) because the dipole limit can only be reached if the inverse momentum transfer is much larger than the diameter of the target. The DWBA results have little similarity with the PWBA ones. In particular, the main maximum ("binary maximum") is massively shifted towards larger angles, and the angular pattern for emission of both electrons to the same side of the beam ("recoil peak region") is quite irregular.

To understand these results, it is useful to refer to the standard semiclassical interpretation according to which "soft collisions" correspond to large impact parameters or angular momenta. Hence high angular momentum partial waves make dominant contributions to the projectile wave functions. Unlike the atomic case, due to the large size of the target these partial waves are still influenced by the effective fullerene potential, so that the plane wave ansatz for projectile states underlying the PWBA is bound to fail. In view of the fact that high angular momentum states are also accessed by the ejected electron, and that there is massive interference between the partial wave amplitudes, it is difficult to extract detailed information from this TDCS. By the same token, this TDCS is rather difficult to calculate using the partial wave approach, hence the DWBA data of Figure 2b contain a larger convergence error (about 15%) than the other data shown.

3.1.2 Ehrhardt geometry, large perturbation

At lower impact energies, the coplanar asymmetric geometry has been used to study the influence of projectile rescattering in the target field by comparing PWBA and DWBA results with experiment (see [40,41] and references therein). Clearly, the exchange amplitude cannot be neglected in this case. The choice of larger scattering angles corresponds to larger momentum transfers. Therefore in the atomic PWBA results the TDCS is concentrated on the binary peak. By contrast, the DWBA predicts a much smaller TDCS in this region, and a relatively large structure in the recoil peak region, which is obviously due to the distorting influence of the target potential on the projectile. These features have indeed been observed experimentally [42].

Again, the results for the jellium shell target have little in common with the hydrogen data. While the binary peak in the DWBA is again significantly smaller than the PWBA one, neither calculation shows any structure of importance in the recoil regime, although the logarithmic plot (see inset) reveals oscillations similar to those seen in

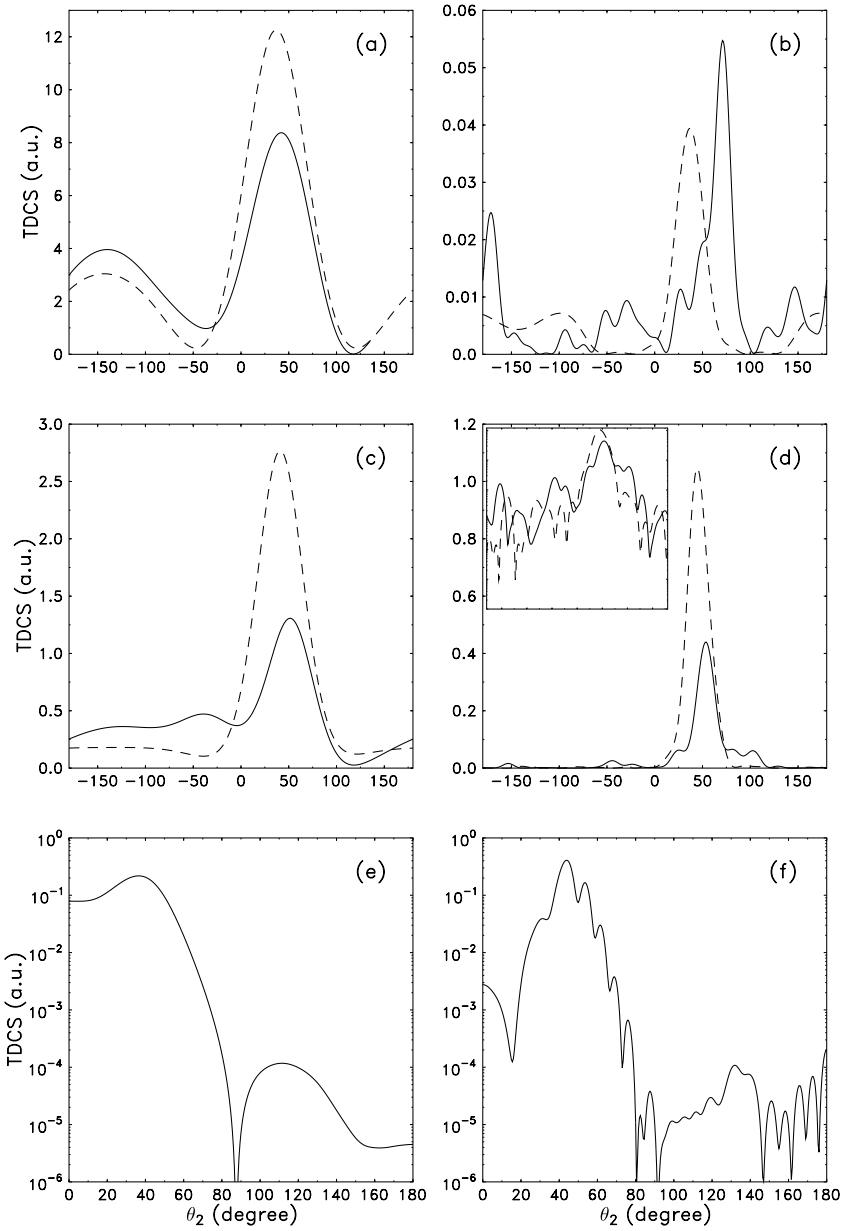

Fig. 2. Comparison between TDCS for $(e, 2e)$ on the $1s$ state of atomic hydrogen (binding energy $E_b = 0.5$ a.u.) and the $1s$ state of the spherical jellium shell model of C_{60} ($E_b = 1.25$ a.u.). In all plots, full curves are results of DWBA calculations, dashed curves represent PWBA data. Top row: coplanar asymmetric geometry, impact kinetic energy $T_0 = 11E_b$, kinetic energy of slow outgoing electron $T_2 = 0.36E_b$, $\theta_1 = -3°$; (a) hydrogen, (b) C_{60}. Middle row: coplanar asymmetric geometry, $T_0 = 4E_b$, $T_2 = 0.5E_b$, $\theta_1 = -15°$; (c) hydrogen, (d) C_{60}. Bottom row: coplanar symmetric energy sharing geometry, $T_0 = 5E_b$, $T_1 = T_2 = 2E_b$; (e) hydrogen, (f) C_{60}.

the soft collision case. Moreover, the binary peak itself is much sharper than in the atomic case.

These observations can be interpreted by noting that the individual electrons are delocalised over the jellium shell. Therefore in relatively hard collisions, where the inverse momentum transfer is smaller than the width of the potential well, the collision is quasi-free, so that the TDCS is essentially determined by the momentum constraint of a free collision. This situation does not occur in atomic physics unless the impact energy is very much larger [43].

3.1.3 Coplanar symmetric energy sharing geometry

In the coplanar symmetric energy sharing geometry, both electrons are detected at the same energy, and at the same angle to the left and right of the incident beam. In this case direct and exchange amplitudes are identical, so that only singlet scattering is possible. Clearly the intrinsically unsymmetric PWBA cannot be valid; in fact the DWBA is the most simple consistent model of this situation. Figures 2e and 2f show DWBA results for this geometry. For atomic targets, the characteristic of this geometry is the presence of a secondary maximum for backward emission of both electron. This feature is due to backscattering of the projectile from the atomic nucleus before the ionizing binary collision between the electrons [44,45]. The calculation for C_{60} predicts only a weak indication of this structure. This is not surprising because in this case there is no well-defined centre of force for the initial collision.

A more remarkable feature is that the oscillatory pattern of the TDCS is much more regular than in the asymmetric situations studied before. This effect is due to the

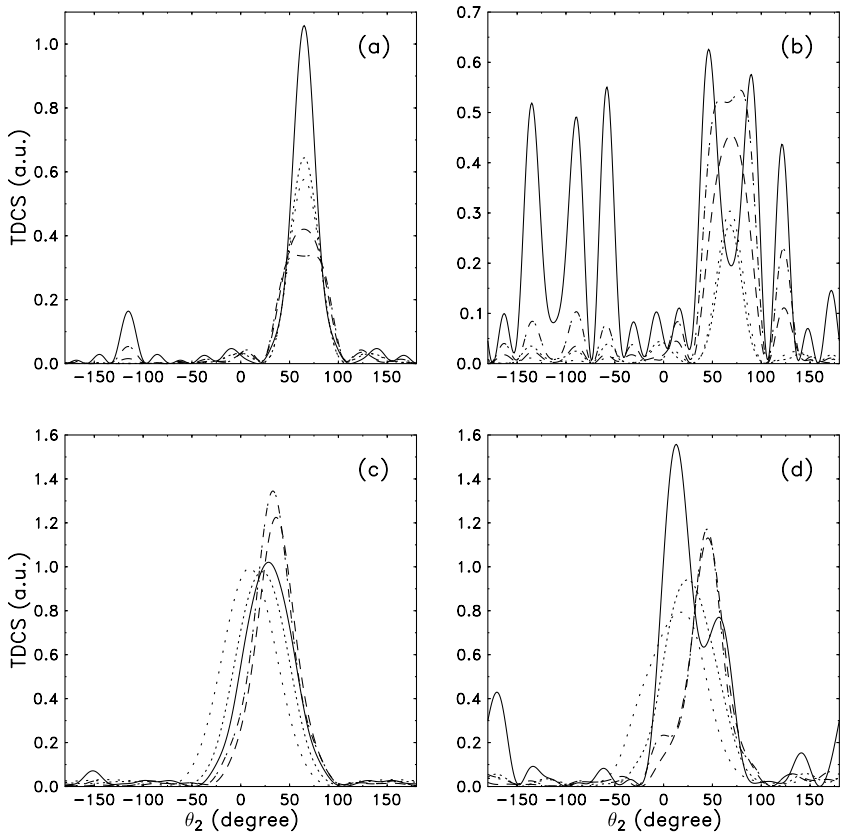

Fig. 3. Triple differential cross-sections for ionisation of the 1s state of the spherical jellium model in the vicinity of the $l = 7$ shape resonance. Impact kinetic energy $T_0 = 234$ eV. Sparsely dotted curve: $T_2 = 1.5$ eV, densely dotted curve: $T_2 = 1.75$ eV, full curve: $T_2 = 2$ eV, dashed curve: $T_2 = 2.25$ eV, dash-dotted curve: $T_2 = 2.5$ eV. Top row: $\theta_1 = -15°$, (a) PWBA, (b) DWBA. Bottom row: θ_1 chosen for each energy T_2 to satisfy bound electron Bethe ridge conditions, (c) PWBA, (d) DWBA.

high symmetry of the kinematics which leads to a more regular interference behaviour of the individual partial wave amplitudes. An attempt to observe the fundamental oscillatory structure of the TDCS for cluster targets predicted in [7] would therefore seem to have the best chance of success if coplanar symmetric energy sharing kinematics are chosen. Notice that a very good energy ($\Delta E < 1$ eV) and angle ($\Delta\theta < 5°$) resolution would be required to successfully conduct such an experiment.

3.2 A note on collective excitations

As was mentioned in the introduction, the inelastic electron-C_{60} scattering cross-section is characterized by energy loss through excitation of plasmons. However upon decay of the plasmon state (or any other relatively long-lived multi-particle excited state) part of the energy transferred to the target may easily be absorbed by any of the plethora of open vibrational channels of the molecule. If a secondary electron is emitted during the decay, it will therefore usually have less energy than an electron emitted in a direct ionisation event.

Accordingly, there will be no significant contribution of collective effects to the $(e, 2e)$ TDCS because the energy-resolved coincident detection of the outgoing electrons selects only those events in which all energy transferred during the collision is taken away by the ionized electron. It is a key advantage of the $(e, 2e)$ technique (underlying in particular the concept of $(e, 2e)$ spectroscopy [2]) that it unambiguously isolates the single-particle reaction channel even in the presence of strong coupling to multi-particle excitation modes.

3.3 Signatures of shape resonances

Experimentally, only one shape resonance at about 3 eV has with certainty been identified in electron attachment experiments. Its jellium shell model representation is the $l = 7$ resonance at 2 eV. This resonance will in the following be used as a representative case in exploring the influence of shape resonances on $(e, 2e)$ TDCS. Figure 3 shows numerical results for TDCS in coplanar asymmetric geometries, where the energy sharing has been varied to sweep over the resonance at a fixed impact energy of 234 eV (other impact energies yield qualitatively the same results).

For an intermediate momentum transfer, the PWBA results (Fig. 3a) show a significant enhancement of the binary peak cross-section and some extra structure in the opposite direction. Allowing for projectile scattering in the effective potential dramatically alters this picture. On the resonance, the TDCS is very much larger than at energies only slightly smaller or larger. It is entirely dominated by the $l = 7$ partial wave of the ejected electron for all emission angles: the shape of the TDCS directly maps the nodal structure of the corresponding Legendre polynomials (Fig. 3b). Thus not only the resonant enhancement

of the ionisation cross-section, but also the angular momentum structure of the resonant continuum state, are directly reflected in the $(e, 2e)$ TDCS. In the PWBA results, these effects are strongly suppressed due to the symmetry with respect the direction of momentum and the associated angular momentum selection rules valid in this approximation. The projectile scattering phases included in the DWBA essentially serve to break this artificial symmetry.

It is instructive to consider the case of bound electron Bethe ridge conditions (vanishing momentum transfer to the target). In this situation, the PWBA requires all ejected electron partial waves to interfere constructively at the binary maximum. This makes the resonant enhancement of the cross-section disappear completely (Fig. 3c). The DWBA has no such constraint, and indeed the $l = 7$ pattern is again clearly visible in the binary peak region (Fig. 3d).

Of course, similar resonance effects could also be studied in other scattering geometries. For example, one could consider coplanar symmetric energy sharing kinematics and adjust the impact energy to give both outgoing electrons an energy corresponding to a single particle resonance. The resulting final state of two electrons "trapped" in the fullerene cage for a relatively long time would of course be highly correlated, so that an independent particle model approach to the study of this interesting situation is clearly inadequate. Therefore, no corresponding DWBA results are shown here.

4 Proposal for a benchmark experiment

This study proposes to exploit the fact that $(e, 2e)$ experiments are particularly sensitive to the single particle continuum states of the scattering system, to investigate the shape resonances in C_{60}. As was shown in the preceding section, massive signatures of the resonant continuum states are to be expected in the $(e, 2e)$ TDCS. However, carrying out corresponding experiments with standard $(e, 2e)$ apparatus would seem to constitute a formidable challenge. It will be argued in the following that a benchmark experiment could be carried out using well-established experimental techniques.

The key problem in any $(e, 2e)$ experiment is the preparation of a sufficiently well-defined and dense target to compensate the smallness of the TDCS. Vos *et al.* [1] circumvented this problem by using a thin film of C_{60} absorbed on a suitable surface. In this high-energy experiment, the sample was irradiated from the back, and surface sensitivity was ensured indirectly by the reduced mean free path of the electrons scattered within the backing substrate. This approach is not available at intermediate energies, where already the primary electrons would be rescattered in the sample. However, the high-resolution EELS measurement of Lucas *et al.* [9] showed that electron scattering on fullerene can also be studied by bombarding a thin film of physisorbed C_{60} and detecting the scattered electrons in specular reflection geometry. Stefani and coworkers have developed an apparatus that combines an energy loss measurement of this type with coincident detection of an ejected electron, and have successfully carried out $(e, 2e)$ experiments on various surfaces systems (see, *e.g.* [46–48]). Therefore, it can be expected that using this reflection geometry $(e, 2e)$ apparatus with a sample prepared as in the thin film experiments discussed before, will directly yield TDCS for intermediate energy $(e, 2e)$ on fullerene.

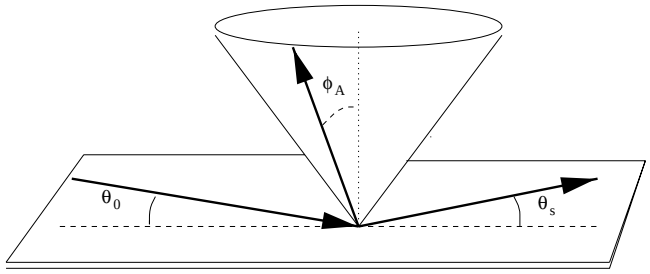

Fig. 4. Sketch of the geometry of the $(e, 2e)$ apparatus used in [46]. The primary electron is detected under the specular angle $\theta_s = \theta_0$, the secondary electron is emitted into a cone with aperture angle Φ_A perpendicular to the surface.

To illustrate this statement, this paper concludes with results of a model calculation for such an experiment. The results of references [1,9] show that it is save to treat the physisorbed C_{60} molecule as if it was actually in the gas phase. Hence the models described in Section 2 can be applied. Figure 4 shows the specific scattering geometry of the Rome apparatus. The electron impinges on the surface under a gracing angle θ_0 and is detected in the specular direction, $\theta_s = \theta_0$. The ejected electron is detected in coincidence with the scattered one if it is emitted into a cone with aperture angle Φ_A. Hence the observed TDCS is integral over this cone. The latter restriction has recently been overcome [47]. However, the cone averaged cross-section is sufficient for the present purpose and therefore preferable to improve statistics.

Figure 4 shows that, speaking in atomic physics $(e, 2e)$ terms, the measurement is carried out in the "recoil regime". Hence the binary ionizing collision must be accompanied by elastic backscattering from the sample. Indeed the work of the Rome group has established that two mechanisms contribute to the TDCS, namely ionisation preceded or followed by elastic scattering from the target [48]. Both mechanisms are modelled in the DWBA approach, whereas only the latter one is included in the PWBA. Therefore only DWBA results are shown in Figure 5. In the ejected electron energy regime considered, the jellium model features two series of shape resonances, starting with $l = 7$ and $l = 12$ respectively. The corresponding scattering phases (without the logarithmic Coulomb contribution) are displayed in the upper part of Figure 5 to indicate the position of these resonances. The lower part of Figure 5 shows that, as expected, distinct signals in the cone integrated triple differential cross-section appear in the vicinity of the resonance energies, in particular for the sharp $l = 7$ and $l = 12$ resonances.

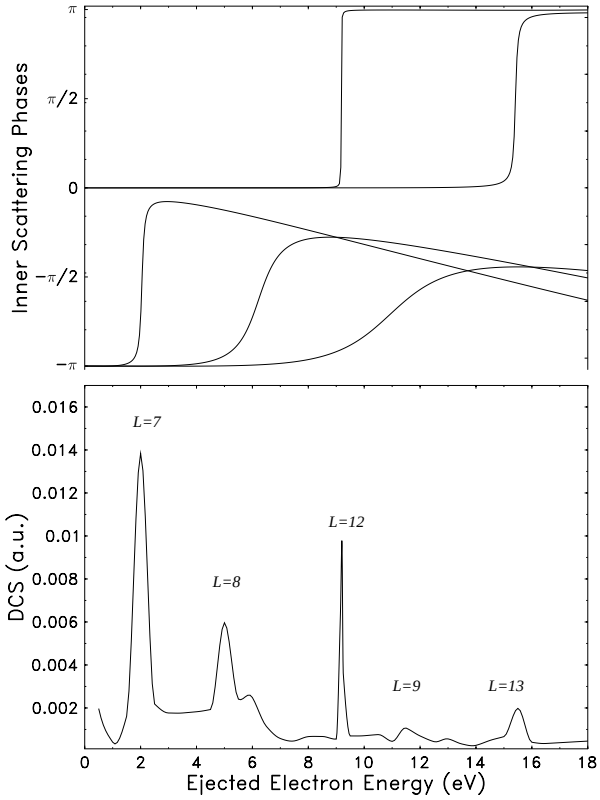

Fig. 5. Top: selected inner scattering phases for elastic electron scattering on C_{60} in the jellium shell model. Bottom: DWBA result for cone-integrated TDCS for $(e, 2e)$ on the $1s$ state of the jellium shell model of C_{60} as function of the secondary electron energy. Scattering geometry as in Figure 4. Impact energy 234 eV, $\theta_0 = \theta_s = 7°$, $\Phi_A = 42.3°$. The resonance structures are labelled with the angular momentum of the resonant partial wave.

5 Concluding remarks

The calculations of jellium shell model TDCS for typical $(e, 2e)$ geometries using the DWBA suggest that $(e, 2e)$ experiments on C_{60} (or other clusters) in coplanar asymmetric geometry might be of limited value, if they are carried out at fixed energies. At small momentum transfers, the enormous number of open angular momentum channels (even in the present simplified model) makes a detailed interpretation of the data extremely difficult. This regime is therefore easier to study using synchrotron radiation. At large momentum transfer, the delocalised electronic states behave essentially as a quasi-free electron gas; this system is more conveniently investigated using a solid (metal) target. The coplanar symmetric energy sharing geometry offers some perspectives for investigating the oscillatory structures of the TDCS if the demanding requirements for energy and angle resolution of the $(e, 2e)$ apparatus can be met. However, it remains to be analyzed to what extend this apparent simplicity is an artifact of the jellium shell approach.

Nevertheless, the coincident detection of scattered and ionized electrons has the potential of becoming a new tool in the study of molecular and cluster targets. The present calculations show that $(e, 2e)$ experiments with fixed impact energy and varying (asymmetric) energy sharing could be used to investigate resonant target continuum states. In this context, the lack of angular momentum selection rules is a distinct advantage over experiments using dipole photons, which could only access a subset of the existing resonant states.

I would like to thank E. Engel for computing the self-consistent jellium sphere model potential. The constructive criticism of the anonymous referees is gratefully acknowledged. The DWBA calculations have been carried out on the heterogeneous workstation cluster of the Frankfurt University computing centre.

Appendix A: Remark on oscillatory structures in scattering cross-sections

As was indicated in the main text, the radial confinement of the delocalised cluster electrons gives rise to oscillatory structures in various scattering cross-sections. However, the mechanisms leading to these oscillations need to be carefully distinguished.

Diffraction-type oscillations in differential electron scattering cross-sections arise when a target characterized by a well-defined length scale is probed with respect to a length scale introduced by the scattering process. The most famous example is high-energy elastic scattering on atomic nuclei which probes the nuclear charge distribution as function of inverse momentum transfer [49]. In $(e, 2e)$ spectroscopy, the principle is the same, but is applied to the wave function as function of recoil momentum [2]. For both types of experiment, standard Fourier analysis shows that the cross-section exhibits oscillations proportional to $\sin^2(k\alpha)$ as function of momentum k when the potential (or wave function) is radially confined to $[0, \alpha)$ in coordinate space. For the case of a jellium shell, the pattern consists of a superposition of two such terms characterized by the inner and outer diameter of the shell.

The oscillations of the total C_{60} photoionisation cross-section as function of photon energy [5] must be of a different nature, because at negligible photon momentum (as is the case for photoionisation in the dipole regime), no additional length scale is involved in the ionisation process. Indeed, Frank and Rost [50] have shown that this effect can be explained by the fact that photoionisation can only take place in the regime of an electron density gradient, *i.e.* at the radial edges of the jellium shell. This leads to a well defined difference ΔR of the total radial path length of electrons ionized at the inner and outer edges of the C_{60} potential well, respectively. In the photoionisation amplitude, the coherent superposition of the corresponding wave functions results in an interference term with a $\cos(k\Delta R)$ dependence on momentum k. This term is responsible for the oscillations seen in the experiment. Since this delicate interference pattern would be masked by any average over momentum transfers to the ejected electron,

it is not surprising that the integrated cross-sections for electron impact ionisation of neutral and ionic fullerenes show no corresponding oscillations [51].

References

1. M. Vos, S.A. Canney, I.E. McCarthy, S. Utteridge, M.T. Michalewicz, E. Weigold, Phys. Rev. B **56**, 1309 (1997).
2. I.E. McCarthy, E. Weigold, Rep. Prog. Phys. **51**, 299 (1988).
3. A. Lahmam-Bennani, J. Phys. B **24**, 2401 (1991).
4. L.G. Gerchikov, P.C. Efimov, V.M. Mikoushkin, A.V. Solov'yov, Phys. Rev. Lett. **81**, 2707 (1998).
5. Y.B. Xu, M.Q. Tan, U. Becker, Phys. Rev. Lett. **76**, 3538 (1996).
6. M. Leuschner *et al.*, Phys. Rev. C **49**, 955 (1994).
7. S. Keller, E. Engel, H. Ast, R.M. Dreizler, J. Phys. B **30**, L709 (1997).
8. B. Barton, E. Eberlein, J. Chem. Phys. **95**, 1512 (1991).
9. A. Lucas, G. Gensterblum, J.J. Pireaux, P.A. Thiry, R. Caudano, J.P. Vigneron, Ph. Lambin, W. Krätschmer, Phys. Rev. B **45**, 13694 (1992).
10. A.W. Burose, T. Dresch, A.M.G. Ding, Z. Phys. D **26**, S294 (1993).
11. N. Ju, A. Bulgac, J.W. Keller, Phys. Rev. B **48**, 9071 (1993).
12. M.J. Puska, R.M. Nieminen, Phys. Rev. B **47**, 1181 (1993).
13. D.A. Gorokhov, R.A. Suris, V.V. Cheianov, Phys. Lett. A **223**, 116 (1996).
14. L.G. Gerchikov, A.V. Solov'yov, J.P. Connerade, W. Greiner, J. Phys. B **30**, 4133 (1997).
15. *Nuclear Physics Concepts in the Study of Atomic Cluster Physics*, edited by R. Schmidt, H.O. Lutz, R.M. Dreizler (Lecture Notes in Physics **404**, Springer, Berlin, 1992).
16. D. Smith, P. Spanel, J. Phys. B **29**, 5199 (1996).
17. O. El Hamidi, J. Pommier, R. Abouaf, J. Phys. B **30**, 4633 (1997).
18. H. Tanaka, L. Boesten, K. Onda, O. Ohashi, J. Phys. Soc. Jap. **63**, 485 (1994).
19. A. Gianturco, R.R. Lucchese, M. Sanna, J. Phys. B **32**, 2181 (1999).
20. A.N. Ipatov, V.K. Ivanov, J.M. Pacheco, W. Ekardt, J. Phys. B **31**, L511 (1998).
21. J.L. Martins, N. Troullier, J.H. Weaver, Chem. Phys. Lett. **180**, 457 (1991).
22. M. Brack, Rev. Mod. Phys. **65**, 677 (1993).
23. R.M. Dreizler, E.K.U. Gross, *Density Functional Theory* (Springer, Berlin, 1990).
24. S. Keller, E. Engel, Chem. Phys. Lett. **299**, 165 (1999).
25. S.T. Manson, L.H. Toburen, D.H. Madison, N. Stolterfoht, Phys. Rev. A **12**, 60 (1975).
26. D.H. Madison, R. Calhoun, W. Shelton, Phys. Rev. A **16**, 552 (1977).
27. F. Salvat, J.M. Fernandez-Varea, W. Williamson, Comput. Phys. Commun. **90**, 151 (1995).
28. A.L. Fetter, J.D. Walecka, *Quantum Theory of Many-Particle Systems* (McGraw-Hill, New York, 1971), Chap. 17.
29. A. Bulgac, N. Ju, Phys. Rev. B **46**, 4297 (1992).
30. J.B. Furness, I.E. McCarthy, J. Phys. B **6**, 2280 (1973).
31. P.A. Lee, G. Beni, Phys. Rev. B **15**, 2862 (1977).
32. F.A. Gianturco, S. Scialla, J. Phys. B **20**, 31 (1987).
33. O. Kroneisen, H.J. Lüdde, R.M. Dreizler, Phys. Lett. A **222**, 405 (1996).
34. V.V. Balashov, in *The Physics of Electronic and Atomic Collisions*, edited by Y. Itikawa *et al.* (AIP conference proceedings 500, AIP, Melville, 2000), p. 319.
35. B. Hafida, P.A. Hervieux, M.E. Madjet, in *XXI ICPEAC book of abstracts*, FR137, Sendai, 1999, p. 688.
36. H. Ehrhardt, K. Jung, G. Knoth, P. Schlemmer, Z. Phys. D **1**, 3 (1986).
37. H.A. Bethe, Ann. Phys. (Leipzig) **5**, 325 (1930).
38. M. Inokuti, Rev. Mod. Phys. **43**, 297 (1971).
39. H. Klar, A.C. Roy, P. Schlemmer, K. Jung, H. Ehrhardt, J. Phys. B **20**, 821 (1987).
40. S. Keller, R.M. Dreizler, L.U. Ancarani, H. Ast, H.R.J. Walters, C.T. Whelan, Phys. Rev. A **59**, 1284 (1999).
41. I. Taouil, A. Duguet, A. Lahmam-Bennani, B. Lohmann, J. Rasch, C.T. Whelan, H.R.J. Walters, J. Phys. B **32**, L5 (1999).
42. M. Brauner, J.S. Briggs, J.T. Broad, T. Rösel, K. Jung, H. Ehrhardt, J. Phys. B **24**, 657 (1991).
43. M. Vos, I.E. McCarthy, Rev. Mod. Phys. **67**, 713 (1995).
44. J.S. Briggs, J. Phys. B **19**, 2703 (1986).
45. X. Zhang, C.T. Whelan, H.R.J. Walters, J. Phys. B **23**, L509 (1990).
46. S. Iacobucci, L. Marassi, R. Camilloni, S. Nannarone, G. Stefani, Phys. Rev. B **51**, 10252 (1995).
47. S. Iacobucci, S. Rioual, A. Ruocco, M. Mastropietro, G. Stefani, J. Phys. IV France **9**, Pr6-145 (1999).
48. A. Ruocco, M. Milani, S. Nannarone, G. Stefani, J. Phys. IV France **9**, Pr6-149 (1999).
49. R. Hofstadter, Ann. Rev. Nucl. Sci. **7**, 231 (1957).
50. O. Frank, J.M. Rost, Chem. Phys. Lett. **271**, 367 (1997).
51. S. Matt, B. Dünser, M. Lezius, K. Becker, A. Stamatovic, P. Scheier, T.D. Märk, J. Chem. Phys. **105**, 1880 (1996).